Journal of ELECTRONIC MATERIALS
https://doi.org/10.1007/s11664-018-6332-4

TOPICAL COLLECTION: 18TH INTERNATIONAL CONFERENCE ON II-VI COMPOUNDS

Clusters of Point Defects Near Dislocations as a Tool to Control CdZnTe Electrical Parameters by Ultrasound

YA.M. OLIKH,[1,4] M.D. TYMOCHKO,[1,5] O.YA. OLIKH,[2] and V.A. SHENDEROVSKY[3]

1.—V.Ye. Lashkaryov Institute of Semiconductor Physics, NAS of Ukraine, 41, pr. Nauky, Kiev 03028, Ukraine. 2.—Faculty of Physics, Taras Shevchenko National University of Kyiv, Kiev 01601, Ukraine. 3.—Institute of Physics, NAS of Ukraine, 46, pr. Nauky, Kiev 03028, Ukraine. 4.—e-mail: jaroluk3@ukr.net. 5.—e-mail: tymochko@ukr.net

We studied the temperature dependence (77–300 K) of the electron concentration and mobility using the Hall method under ultrasound (the acoustic Hall method) to determine the mechanisms by which ultrasound influences the electrical activity of near-dislocation clusters in *n*-type low-ohmic $Cd_{1-x}Zn_xTe$ single crystals ($N_{Cl} \approx 10^{24}$ m^{-3}; x = 0; 0.04) with different dislocation density (0.4–5.1) $\times$ 10^{10} m^{-2}. Changes in electrophysical parameters were found to occur as a function of temperature and ultrasound intensity. To evaluate the relative contribution of different charge carrier scattering mechanisms (lattice scattering, ionized impurity scattering, neutral impurity scattering, and dislocation scattering) and their change under ultrasound, a differential evolution method was used. This method made it possible to analyze experimental mobility $\mu_H(T)$ by its nonlinear approximation with characteristic temperature dependence for each mechanism. An increase in neutral impurity scattering and a decrease in ionized impurity and dislocation scattering components were observed under ultrasound. The character and the amount of these acoustically induced changes correlate with particular sample dislocation characteristics. It was concluded that the observed effects are related to the acoustically induced transformation of the point-defect structure, mainly in the near dislocation crystal regions.

Key words: CdZnTe crystals, ultrasound, dislocation clusters, Hall effect

INTRODUCTION

$Cd_{1-x}Zn_xTe$ (CZT) crystals are basic semiconductors used for radiation detection. Their widespread use is limited by bulk defects, including dislocations, blocks, inclusion, and point defect (PD) complexes, that strongly affect carrier transport and the consequent detector performance.[1–3] Moreover, in addition to Te particles, dislocation clusters have been reported to cause electric field perturbations and related non-uniformities.[3–7] Therefore, to achieve improved material properties, dislocations and interactions between dislocations and other defects in CZT crystals must be understood and controlled.

However, studies to date have focused primarily on electrical (EPh) and photoelectrical (PhE) properties related to PD compensation.[5–9] The participation of active near-dislocation clusters (NDC) has received limited attention. Direct methods for NDC electrical activity studies are unavailable. However, the Hall method under ultrasound (the acoustic Hall dynamic method) holds potential for the complex electrically active dislocation systems in semiconductor structural studies.[10–12] Taking into account the high density of dislocations ($N_{Dis} \sim 10^{10}$ m^{-2}), A_2B_6 compounds that are especially acoustically sensitive are unique in terms of their compact correlation of changes in electronic and dislocation systems and can serve as exemplary model

(Received December 1, 2017; accepted April 25, 2018)

Published online: 15 May 2018

materials for the study of acoustic–dislocation–electron interaction in semiconductors.[10,13,14] The intense ultrasound wave causes dislocation vibrations. In fact, for ultrasound intensities $W_{US} \sim 10^4$ W m^{-2} and $N_{Dis} \sim 10^{10}$ m^{-2}, the entire volume of the crystal is in a state of oscillatory deformation, and the reorganization of defects occurs throughout the sample volume. The main processes involved in long-term ultrasound load include the "capture" or "freeing" of mobile electrically active PDs (acceptors or donors) from dislocations that are "drains" (traps) for PDs. In experiments, depending on the state of the impurity-defect structure and ultrasound parameters, as well as residual changes, temporary changes can only be realized under ultrasound. The most informative method for deciphering the mechanisms of this phenomenon is dynamic—i.e., *in situ*—research. Moreover, the complex impurity-defect structure of A_2B_6 crystals under ultrasound can be labile, even at low temperatures (< 300 K).[13,14]

Because all acoustic energy is spent under US loading, the oscillatory motion of the dislocations in the crystal[9,15] and the changes in the EPh parameters observed are associated with certain rearrangements in the structure of the PD and their complexes. Thus, the dislocations are the main mediators of US energy transfer to the electrically active PD. Moreover, these complexes should be located near the dislocations, preferably in the NDC regions, which are actually swept by dislocations in the process of their forced acoustically induced (AI) oscillations.

In this context, the following questions arise: (1) Can such structural imperfection in real crystals of $Cd_{1-x}Zn_xTe$ be used to control their EPh and PhE characteristics by ultrasound? (2) What is the nature of such AI changes? To clarify the specific mechanisms of AI changes and the features that depend on the output EPh and the material structure characteristics in low-ohmic crystals of the *n*-type $Cd_{1-x}Zn_xTe$ ($N_{Cl} \approx 10^{24}$ m^{-3}, $x = 0$; 0.04) with various dislocation densities $(0.4–5.1) \times 10^{10}$ m^{-2} the temperature dependence (77–300 K) and acoustic Hall effect were studied.

EXPERIMENTAL SAMPLES AND TECHNIQUE

The results obtained for four samples are presented herein: CdTe (nos. 1, 2 and 4) and $Cd_{0.96}Zn_{0.04}Te$ (no. 3), whose main EPh parameters are given in Table I. All crystals except no. 1 were fabricated using the vertical Bridgman method at a low cadmium vapor pressure in an ampoule.[16] Single crystal no.1 was grown in an atmosphere of Cd (up to 2 atm). Sample nos. 2, 3 and 4 were doped with chlorine ($N_{Cl} \approx 10^{24}$ m^{-3}). Sample no. 1 is undoped, the main point defects being background impurities (in particular, copper[17]) and intrinsic defects. The interstitial Cd_i is responsible for the *n*-type conductivity of crystal no. 1, and the replacement of tellurium Cl_{Te} with chlorine is responsible for *n*-type conductivity in crystal nos. 2, 3 and 4. The ohmic contacts on the samples ($\sim (1 \times 3 \times 10)$ mm^3) were formed by thermal deposition of indium in a vacuum at 175°C. The concentration of charge carriers n and mobility μ in the temperature region (77–300 K) were determined by the Hall method in the regime of dc electric and magnetic fields. The n and μ under US (the acoustic Hall method) were measured in a liquid nitrogen cryostat equipped with acoustic elements. The cryostat construction allowed measurements to be carried out sequentially for the same sample with its impurity-defect system in the initial or acoustically perturbed state.[9–11]

A longitudinal US wave with a frequency of about 10 MHz and an intensity up to 10^4 W/m^2 was introduced into the sample through a buffer plate from a piezoelectric transducer (a $(Y + 36°)$-cut lithium niobate plate) fed with a sinusoidal signal of a high-frequency generator (see the diagram of the acoustic unit in the inset in Fig. 1). The relative change in accuracy for the measurement of electric signals under ultrasound loading reached 2%, and that for temperature was about 0.1 K. The accuracy of the Hall coefficient R_H and the conductivity σ calculation is 3–5%. The temperature variation of the sample under intensive US loading during the course of measuring a separate experimental point did not exceed 2 K.

To control the structure quality of experimental samples, the method of x-ray topography was used. For satellite samples made from the same ingot as Hall samples at cleaved planes with orientation (110), the reflections (220) and (440) were analyzed by high-resolution x-ray diffraction. To evaluate the dislocation density, the Williamson–Hall construction and the formula containing the magnitude of the Burgers vector b for screw dislocations and angle β of the Williamson–Hall construction $N_{Dis}^{XR} = \beta^2/4{,}35b^2$ were used.[18,19] The results pertaining to the state of the crystal lattice of the samples, namely, the deformation of the lattice ε_c and the density of the screw dislocations N_{Dis}^{XR}, are given in Table I. Since the screw dislocations in $Cd_{1-x}Zn_xTe$ are much less mobile than the edge dislocations, they have a higher density.[20] Note that in our case, the ultrasound does not interact solely with screw dislocations, whose concentration is estimated from x-ray studies. Of course, AI restructuring of PD complexes occurs in the deformation vicinity of all dislocations (screw and edge) where impurity-defect complexes are localized.[15] The resulting N_{Dis}^{XR} and ε_L data indicate only the relative degree of structure perfection for the selected set of samples.

RESULTS

We found that the detected AI changes in the Hall coefficient R_H and the conductivity σ are reversible.

Table I. The electrophysical parameters of the experimental $Cd_{1-x}Zn_xTe$ samples

Parameters samples	CdTe no. 1		CdTe no. 2		$Cd_{0.96}Zn_{0.04}Te$ no. 3		CdTe no. 4	
Dopant impurity N_i (m^{-3})	–		$N_{Cl} \approx 10^{24}$		$N_{Cl} \approx 5 \times 10^{24}$		$N_{Cl} \approx 5 \times 10^{23}$	
N_{Dis}^{XR} (10^{10} m^{-2})	0.4		1		3.4		5.1	
Lattice deformation ε_c (10^{-4})	1.02		1.86		7.13		11.74	
US loading (~ 10 MHz, 10^4 W/m^2)	**0**	**US**	**0**	**US**	**0**	**US**	**0**	**US**
n (10^{21} m^{-3})								
300 K	0.58	0.58	31.69	31.95	171	175	31.9	32.4
100 K	0.41	0.48	23.8	31.92	70.6	72.2	22.9	27.0
μ_H (m^2/V s)								
300 K	0.079	0.078	0.084	0.079	0.077	0.076	0.065	0.064
100 K	0.32	0.22	0.192	0.123	0.077	0.085	0.063	0.075

N_i—impurity concentration, N_{Dis}^{XR}—the screw dislocation density, ε_c—lattice deformation, n and μ are charge carrier concentration and mobility, respectively. The n and μ values in the columns with "0" symbols correspond to the initial samples, and "US" symbols denote samples under ultrasound loading $W_{US} \approx 10^4$ W/m^2.

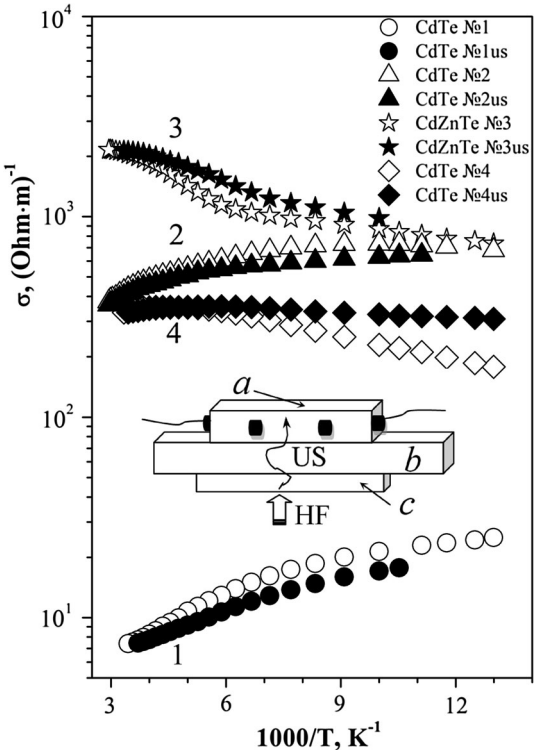

Fig. 1. Temperature dependence of the conductivity $\sigma(T)$ in $Cd_{1-x}Zn_xTe$ samples (sample numbering according to the Table I). In all figures, curves with unfilled symbols correspond to initial samples, and curves with filled symbols correspond to ultrasound loading ($W_{US} \approx 10^4$ W/m^2). The inset demonstrates the scheme of an acoustical unit: sample (a), buffer (b), piezoelectric transducers (c), high frequency (HF), longitudinal ultrasound wave (US).

When the ultrasound was switched off and the acoustic action terminated, the sample parameters returned slowly (50–500 s) to their initial values depending on the temperature and the US intensity. Figures 1, 2, and 3 show the values of relaxed (stable) parameters. The peculiar relaxation characteristics of $\sigma(t)$ (when the ultrasound is switched on and off in one of the samples) have been described in greater detail.[13,14]

Temperature Dependence of Conductivity $\sigma(T)$

Figure 1 shows the temperature dependence of the initial sample before and during US loading. In the latter case, the change in $\sigma(T)$ is small at room temperature. However, when the temperature is lowered, the relative modifications reach ~ 30%. The change in $\sigma(T)$ as a function of temperature and AI change differ between samples: $\sigma(T)$ decreases both with increasing T and under US loading for sample nos. 1 and 2, while the AI changes have the opposite effect, as $\sigma(T)$ increases with increasing T and under US loading for sample nos. 3 and 4 with higher density N_{dis}^{XR}.

Temperature Dependence of Charge Carrier Concentration $n(T)$ and Mobility $\mu_H(T)$

To understand the mechanism by which the conductivity under ultrasound changes, it is crucial to distinguish AI modifications associated with the variations in the concentration and mobility of charge carriers. This can be done by Hall effect measurements.[21,22] The relevant results for 300 K and 100 K are given in Table I.

Figure 2 shows the temperature dependence of the electron concentration $n(T)$. Slight changes in $n(T)$ are observed for all samples; the shallow donor level considered to result from interstitial Cd atoms in sample no. 1 and chlorine in place of Te in sample nos. 2, 3 and 4 is depleted in the region of 77–300 K.[22,23] However, for sample no. 3 in the high-temperature region, there is a slight increase in $n(T)$. Under US, $n(T)$ increases slightly (to ~ 10%) for all samples; in addition, it rises when the temperature decreases. The inset demonstrates

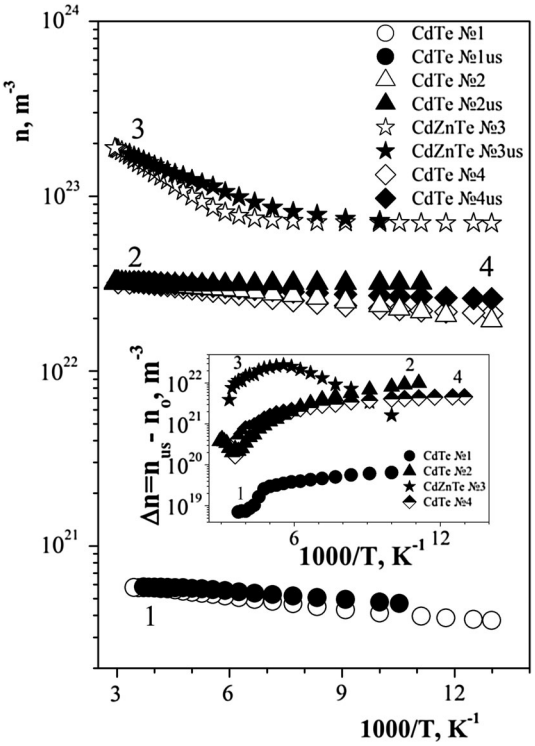

Fig. 2. Temperature dependence of charge carrier concentration $n(T)$ in $Cd_{1-x}Zn_xTe$ samples (sample numbering according to Table I); empty symbols = without ultrasound, filled symbols = under ultrasound loading ($W_{US} \approx 10^4$ W/m^2). The inset demonstrates the temperature dependence of the acoustically induced difference in electron concentration: under the ultrasound loading minus without ultrasound $\Delta n_{US}(T) = (n_{US}(T) - n_0(T))$.

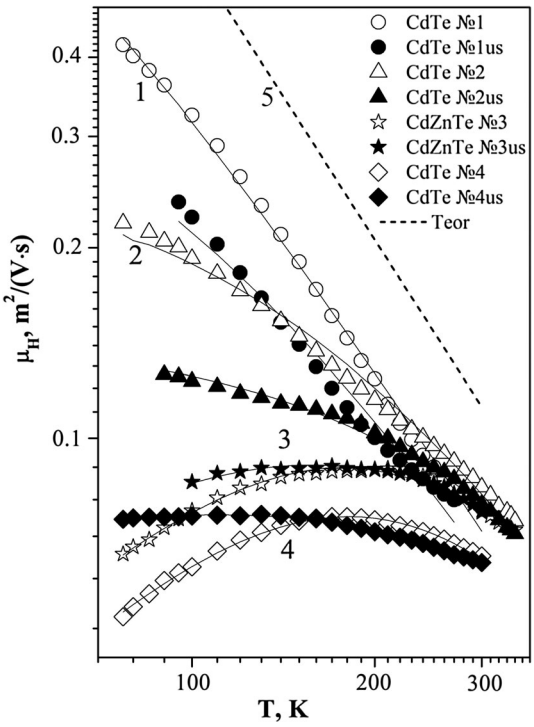

Fig. 3. Temperature dependence of charge carrier mobilities $\mu_H(T)$ in $Cd_{1-x}Zn_xTe$ samples (numbering curves according to the Table I); empty symbols—without ultrasound, filled symbols—under ultrasound loading ($W_{US} \approx 10^4$ W/m^2). Symbols correspond to experimental data, and curves were fitted to the results of the calculations by way of nonlinear approximation (see Table II). Dashed curve 5 demonstrates the theoretical temperature dependence of mobility for the optical-phonon scattering mechanism $\mu_{po}(T)$ in CdTe crystals.[29]

the temperature dependence of the AI difference in electron concentration: under ultrasound minus without ultrasound $\Delta n_{US}(T) = (n_{US}(T) - n_0(T))$.

Figure 3 shows the experimental dependence of electron mobility $\mu_H(T)$. The temperature-dependent and AI changes in $\mu_H(T)$ differ significantly for all samples. The US reduced $\mu_H(T)$ over the entire temperature range, reaching 50% reduction at 100 K for sample nos. 1 and 2. The nature of the influence of US for sample nos. 3 and 4 with low mobility values is more complicated and depends on the temperature range: (a) at high temperature ($T > 200$ K), the AI decrease of $\mu_H(T)$ is similar to that observed for sample nos. 1 and 2 with high mobility values; however, it is insignificant (5%); (b) at the same time, an increase in $\mu_H(T)$ is observed (for $\sim$ 10–15%) and the dependence of $\mu_H(T)$ is saturated at low temperature ($T < 150$ K).

In Fig. 4, to clarify the results of the US action, we show the difference characteristics of $\Delta\mu_{US}^{-1}(T) = (1/\mu_{US}(T) - 1/\mu_0(T))$ determining the AI changes in the electron scattering efficiency. The non-monotonic character of $\Delta\mu_{US}(T)$ for all samples suggests at least two qualitatively different mechanisms for the AI effects, one of which predominates at high temperature ($T > 200$ K), and the other at low temperature ($T < 150$ K).

DISCUSSION

General Character of the Current Flow in the Initial Samples

To understand the nature of the US action, one must know the detailed mechanisms of current flow in the sample. Taking into account the screw dislocation density N_{Dis}^{XR} (Table I), we suppose the dislocations to be the main traps for PD in our samples.[1,4,12,20,24] A high concentration of dopant ($N_{Cl} \approx 10^{24}$ m^{-3}) at the annealing stage contributed to the formation of PD clusters, especially around dislocations. In fact, the processes of cluster and dislocation formation are interrelated. Not only does PD clustering occur at the dislocation, but dislocations are also formed around large Te precipitates.[1,20,25] The regions of the electric field around the heterogeneities are considered impenetrable by electrons. Therefore, the effective dimensions of the crystal and the calculated $\mu_H(T)$, respectively, are underestimated.[3,6,7,26] As the following experimental results show, in our samples, the processes of current transfer and the effects of ultrasound are not strictly defined by isolated point defects, but by structure inhomogeneities resulting from admixture aggregates.

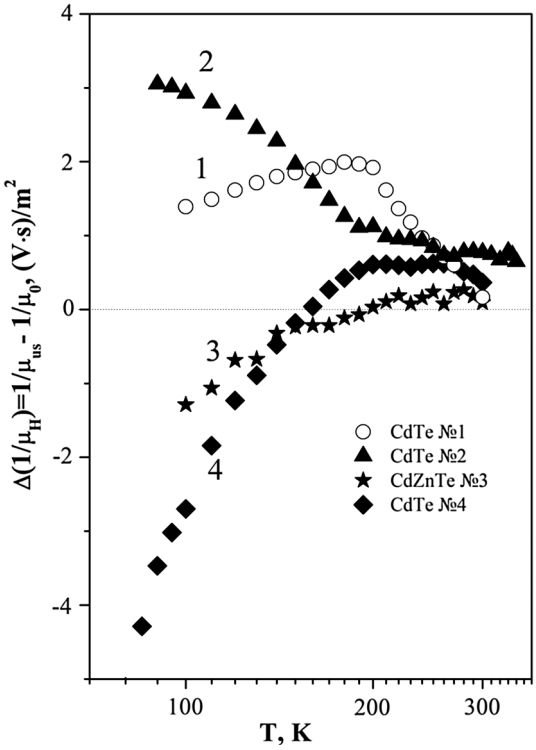

Fig. 4. Temperature dependence of acoustically induced reverse carrier mobility difference: under the ultrasound loading minus without it $\Delta\mu_{US}^{-1}(T) = (1/\mu_{US}(T) - 1/\mu_0(T))$. Numbering curves according to numbering samples are presented in Table I.

Nonlinear Approximation $\mu_{exp}(T)$ Within a Homogeneous Sample Model

The dominant mobility scattering mechanism for bulk crystals of CdZnTe is considered to be lattice scattering via deformation potential, piezoelectric coupling, and non-phonon scattering such as ionized impurity scattering, neutral impurity scattering, and dislocation scattering.[2,4–7,26,27] Because the mobility of electrons due to piezoelectric potential scattering is higher than 10^2 m^2/V s, it is not taken into account.[2] Therefore, the temperature dependence of the reciprocal of the mobility μ^{-1} according to Matthiessen's rule[4,22,28] is given by:

$$1/\mu = 1/\mu_N + 1/\mu_{dis} + 1/\mu_{ii} + 1/\mu_{Lat}, \quad (1)$$

where μ_N, μ_{dis}, μ_{ii} and μ_{Lat} are neutral impurity scattering, dislocation scattering, ionized impurity scattering, and lattice mobility scattering components, respectively. The temperature dependence of these mechanisms is described as follows[21–23,29]:

$$\mu_N = a_N T^0 \quad (2')$$

$$\mu_{dis} = a_{dis} T \quad (2'')$$

$$\mu_{ii} = a_{ii} T^{3/2} \quad (2''')$$

$$\mu_{Lat} = a_{Lat} T^{-3/2} \quad (2'''')$$

Assuming that $\mu_H^{exp}(T)$ for all samples, both output and US loaded, is also determined by these scattering mechanisms, we can write:

$$\mu_H^{exp}(T) = \left(1/a_N T^0 + 1/a_{dis} T + 1/a_{ii} T^{3/2} + 1/a_{Lat} T^{-3/2}\right)^{-1} \quad (3)$$

To clarify the mechanism of the US action at $\mu_H^{exp}(T)$ for all samples, it is important to estimate the relative contribution of each of the scattering mechanisms for charge carriers. To do this, we have approximated experimental $\mu_H^{exp}(T)$ according to (3). For such a nonlinear approximation we used the differential evolution method, as it is one of the calculation approaches imitating natural processes.[30,31] The results of these calculations are given by the solid lines in Fig. 3. This method can satisfactorily describe our $\mu_H^{exp}(T)$ for all samples, both output and US loaded. The values of the corresponding a_N, a_{dis}, a_{ii}, and a_{Lat} coefficients, which were considered as search parameters, are given in Table II.

Approximation Results for $\mu_H^{exp}(T)$ Showed

Neutral Impurity Scattering

Taking into account the formula for $\mu_N(T)$[32–34] and the above ratio $\mu_N = a_N T^0$, we can write that

$$a_N = \frac{q^3}{80\pi N_n \hbar^3} \cdot \frac{m^*}{\varepsilon\varepsilon_0} \quad (4)$$

where q is the electron charge, $m^* = 0.11m_0$ is the electron effective mass, ε_0 is the dielectric constant, $\varepsilon = 10.6$ is the CdTe dielectric constant, $\hbar$ is the reduced Planck constant, and N_N is the neutral impurity concentration. Using the given q, m, ε values and the calculated value of a_N from approximation (4), we calculate N_N; the results are also given in Table II. We can see that N_N increases with US for all samples. Specifically, the scattering on neutral impurities increases. Moreover, there is a correlation between the magnitude of N_N and the dislocation structure of the samples: an increase in both the absolute values of N_N and their AI increase ΔN_N^{US} is observed for samples with larger N_{Dis}^{XR}.

Dislocation Scattering

Dislocations can be regarded as scatterers and charged inclusions modulating the potential of the crystal lattice. The perturbation of the lattice by dislocations is described by the deformation potential. In this case, $\mu_{dis} = a_{dis}T$. The following formula is used for the component of dislocation scattering mobility[22,32–34]:

$$\mu_{dis} = \frac{30\sqrt{2\pi\varepsilon\varepsilon_0}\varepsilon\varepsilon_0 c^2 k_B T\sqrt{n}}{q^2 N_{dis} f^2 \sqrt{m^*}} \quad (5)$$

where $c = 6.48$ Å is the base lattice CdTe constant, k_B—is the Boltzmann constant, f is the fraction of

Table II. Results of approximation for experimental dependence $\mu_H^{exp}(T)$ for $Cd_{1-x}Zn_xTe$ samples

	CdTe no. 1		CdTe no. 2		$Cd_{0.96}Zn_{0.04}Te$ no. 3		CdTe no. 4	
Samples parameters	**0**	**US**	**0**	**US**	**0**	**US**	**0**	**US**
a_N (m^2/V s)	2.42	0.47	0.31	0.15	0.33	0.17	0.26	0.09
N_N (10^{22} m^{-3})	0.6	3.2	4.9	9.9	4.5	8.9	5.7	16.4
ΔN_N^{US} (10^{22} m^{-3})	2.6		5.0		4.4		10.7	
a_{dis} (10^{-4} m^2/V s K)	–	–	–	–	11.4	20.9	11.6	123
$N_{dis}{\cdot}f^2$ (10^{12} m^{-2})	–	–	–	–	17.7	9.8	7.5	0.7
$N_{dc}=(N_{dis}{\cdot}f^2)/c$ (10^{22} m^{-3})	–	–	–	–	2.7	1.5	1.2	0.1
ΔN_{dc}^{US} (10^{22} m^{-3})	–		–		– 1.2		– 1.1	
a_{ii} (10^{-4} m^2/V s $K^{-3/2}$)	91	532	45.2	39.6	–	–	5.3	17.1
N_{ii} (10^{22} m^{-3})	0.17	0.03	0.78	0.99	–	–	6.58	2.16
ΔN_{ii}^{US} (10^{22} m^{-3})	– 0.14		0.21		–		– 4.42	
a_{Lat} (10^2 m^2/V s $K^{3/2}$)	3.8	3.9	6.1	8.7	7.5	9.8	6.1	11.5
Δa_{Lat}^{US} (10^2 m^2/V s $K^{3/2}$)	0.1		2.6		2.3		5.4	

a_N, a_{dis}, a_{ii}, and a_{Lat} are coefficients of the decomposition in T degrees; N_N is the neutral impurity concentration, $\Delta N_N^{US} = N_N^{US} - N_N^0$; N_{dis}—dislocation density per unit area, f is the fraction of filled traps ($0 \le f \le 1$), $N_{dc}=(N_{dis}{\cdot}f^2)/c$ is the concentration of dislocation centers, $\Delta N_{dc}^{US} = N_{dc}^{US} - N_{dc}^0$; N_{ii} is the concentration of ionized impurities, $\Delta N_{ii}^{US} = N_{ii}^{US} - N_{ii}^0$; $\Delta a_{Lat}^{US} = a_{Lat}^{US} - a_{Lat}^0$.

filled traps, T is the absolute temperature, n is the screening carrier concentration and N_{dis} is the dislocation density per unit area. Taking into account this formula and considering the ratio (2″) $\mu_{dis}= a_{dis}T$, we can write:

$$a_{dis} = \frac{30\sqrt{2\pi\varepsilon\varepsilon_0}\varepsilon\varepsilon_0 c^2 k_B\sqrt{n}}{q^2 N_{dis} f^2\sqrt{m^*}} \qquad (6)$$

Using (6) and the a_{dis} values found from the approximation, we calculate $N_{dis}{\cdot}f^2$, and the results are shown in Table II. One can see μ_{dis} manifests only for sample nos. 2 and 3, with high N_{Dis}^{XR} and with $N_{dis}{\cdot}f^2$ decreasing after US loading. Specifically, the overall dislocation scattering component is reduced.

As the values $N_{dis}{\cdot}f^2 \sim 10^{12}$ m^{-2} for all samples are too large and not agree with the data of topographic measurements (N_{Dis}^{XR}, see Table I), it is necessary to clarify their possible physical origin. The values of $N_{dis}{\cdot}f^2$ may correspond to the walls of dislocation cells with very high dislocation density.[35] Similar quantities of $N_{dis} \sim 10^{12}$ m^{-2} are also realized in the near-contact and near-surface regions of the sample.[34–36] In the context of this consideration of the acoustic–dislocation interaction, it will be appropriate to assume that the mathematically calculated values of $N_{dis}{\cdot}f^2$ are meaningful beyond the dislocation concentration. Indeed, dividing $N_{dis}{\cdot}f^2$ by a lattice constant c, we obtain the concentration of scattering centers $N_{dc} = (N_{dis}{\cdot}f^2)/c$, thereby identifying the dislocation cluster as a local region of deformation and electric fields.

We'll assume that N_{dc} corresponds to the concentration of electron traps in the depositional regions of the crystal. The conclusion follows that values of $N_{dis}{\cdot}f^2$ ($\sim 10^2$ larger than N_{Dis}^{XR}) reflect the main features of the dislocation scattering mechanism for charge carriers in CdTe crystals. Specifically, scattering does not occur by separate dislocation, but generally occurs by NDC containing a high concentration of deformation centers N_{dc}. This feature of the dislocation mechanism for the scattering of charge carriers, and the fact that the quantitative characteristic is not N_{dis}, but the amount of N_{dc} in the volume swept by dislocations in their oscillations in the US field, eliminates the seemingly fundamental discrepancy with the previously established fact that the presence of dislocations with densities up to $N_{dis} \sim 10^{12}$ m^{-2} does not directly affect the motion of carriers in semiconductor crystals.[25,33] Malyk and Syrotyuk[37] reached a similar conclusion about the crucial contribution of the scattering component of charge carriers at the potential of static deformation (CD component) to $\mu_H(T)$ in CdTe crystals. It should be mentioned that Pekar[3] considered the dislocations as charged inclusions when analyzing mobility in heterogeneous semiconductors. The electrostatic dislocation field contributes significantly to the diffusion of the carrier motion and contributes to the mobility reduction more than the deformation potential. Therefore, the effective mobility $\mu_H= \mu_0(1 - \Delta)$.

Ionized Impurity Scattering

As a rule, the Brooks–Herring formula is used to calculate the mobile component due to scattering on ionized impurities[29]:

$$\mu_{ii} = \frac{4\left(\frac{2}{\pi}\right)^{\frac{3}{2}}(kT)^{\frac{3}{2}}(4\pi\varepsilon_0\varepsilon)^2}{q^3 m^{*\frac{1}{2}} N_{ii}[\ln(b)-1]} \tag{7}$$

where

$$b = \frac{6m^*(kT)^2(4\pi\varepsilon_0\varepsilon)}{\pi q^2\hbar^2 n} \tag{8}$$

Here N_{ii} denotes the concentration of ionized impurities, and n is electron concentration. Under these conditions, which are valid for all the samples described herein, the scattering coefficient on ionized impurities takes the form

$$a_{ii} = \frac{4\left(\frac{2}{\pi}\right)^{\frac{3}{2}}k^{\frac{3}{2}}(4\pi\varepsilon_0\varepsilon)^2}{q^3 m^{*\frac{1}{2}} N_{ii}\left[\ln\left(\frac{6m^*(kT)^2(4\pi\varepsilon_0\varepsilon)}{\pi q^2\hbar^2 n}\right)-1\right]} \tag{9}$$

Through (9), and from the approximated magnitudes of a_{ii}, we calculate N_{ii}, and the results are given in Table II. The concentration of ionized impurities decreases under US for sample nos. 1 and 4. For sample no. 2, N_{ii} under US increases slightly, and for no. 3, N_{ii} is not found from the approximation.

Phonon Lattice Scattering

The scattering mobility component due to scattering on optical phonons μ_{po}has been evaluated. According to,[29] this component can be given as $\mu_{po} = \mu_F\Phi$, where

$$\mu_F = \frac{q}{2\alpha_e\omega_1 m_e^*}\left(e^{\frac{\hbar\omega_1}{k_B T}}-1\right), \tag{10}$$

α_e= 0.38 is the polaron coupling constant, $\omega_1 = 2.63 \times 10^{13}$ rad/s is optical modes oscillation frequency of CdTe. At low temperature $\Phi \sim 1$, at high temperature $\Phi \sim 8/3(\pi\hbar\omega_1/kT)^{-1/2}$. As $\frac{q}{2\alpha_e\omega_1 m_e^*} = 0.0757$ m^2/W s, we obtain for CdTe $\mu_{po} = 5.8 \times 10^2 T^{-3/2}$.

As is shown in Table II, a_{Lat}= (3.8–19.6) $\times 10^2$ m^2/W s K$^{3/2}$ obtained from the $\mu_H^{exp}(T)$ approximation for our samples differ from a_{po}. From this it follows that the obtained a_{Lat} is a compound function of various scattering components on lattice vibrations, including those by optical, acoustic phonons, deformation potential, and piezopotential. Therefore, unfortunately, we can not explicitly separate these contributions and evaluate the detected AI changes of individual components. However, in general, a_{Lat} is satisfactorily implemented to the approximation curves and $\mu_H^{exp}(T)$, and it also shows a correlation with the sample dislocation structure. An increase in both a_{Lat} and Δa_{Lat}^{US} is observed as the N_{Dis}^{XR} increases.

Summarizing the Consideration of the Approximation Results

What is Common for all the Samples Under Ultrasound?

N_N increases, that is, scattering increases on neutral impurities. Moreover, there is a correlation between N_N and sample dislocation structure, namely, the increase in both the absolute values of N_N and their AI increase ΔN_N^{US} for samples with larger N_{Dis}^{XR}. This may be due to the recharge (ionization) of certain centers (see below), as well as the disintegration of more complex systems. It is also likely that ΔN_N^{US} characterizes not only the AI change in the concentration of neutral impurities, but also the change in the integral (total) contribution of electron scattering on neutral impurity complexes. That is, during AI forced oscillations, scattering on these complexes increases, and this manifests formally as an increase in N_N.

What is Distinct, Taking into Account the Features of the Dislocation Defect Structure of Samples?

Compare the results of approximation for sample nos. 2 and 4 which exhibit similar initial doping levels, magnitudes, and temperature-dependent changes in carrier concentration. They have similar mobility at the HT (Table I). At the same time, the samples differ with respect to their initial dislocation structure and the nature of the temperature-dependent and AI mobility changes. For sample no. 4, the scattering on the ionized impurities and multiple ($N_{ii} \sim 6.6 \times 10^{22}$ m^{-3} and $N_{dc} \sim 1.2 \times 10^{22}$ m^{-3}) deformation centers of the NDC is determinative. The ultrasound reduces these scattering components. As a result, an increase in μ_{exp} at low temperature occurs. For sample no. 2, where the scattering component on N_{dc} is not observed, scattering on ionized impurities is less pronounced ($N_{ii} \sim 10^{22}$ m^{-3}); in this case, the effect of ultrasound does not lead to an increase in mobility, but instead, under US, μ_{exp} decreases throughout the entire temperature range. At the same time, according to the results of approximation, scattering on ionized impurities increases to a certain extent. However, the determinative AI effects are the change in scattering on neutral impurities and phonons of the lattice, namely, the growth of N_N and a_{Lat}.

Let us consider sample nos. 1 and 3, whose defect structure, especially with respect to dislocation density, is significantly different. The effect of ultrasound is also different. For the initial sample no. 1, a certain insignificant contribution of N_{ii} scattering was found to decrease with US. However, here an alternative mechanism, the AI growth of

scattering on neutral impurities, accounts for the significant AI μ_{exp} decrease For sample no. 3, the scattering component on N_{ii} does not formally appear. However, the AI scattering on N_{dc} is significantly reduced.

To understand the ambiguity associated with the estimated contribution made by each of the scattering mechanisms on N_{ii} and/or N_{dc}, it is necessary to clarify the nature of their competitive manifestation in our calculations. When the temperature dependence of the mobility components of μ_{dis} and μ_{ii} converge, they cannot be separated by the computer approximation used. For example, for sample no. 3 (compared to other samples), there is an evident temperature change in the electron concentration $n(T)$ that, as can be seen from the Brooks–Herring formula (7), slightly weakens the temperature course of $\mu_{ii}(T)$, which no longer corresponds to $\sim T^{3/2}$, but $\sim T^{r}$, where $r \approx 1$. Therefore, in this case, the large magnitudes of N_{dc} obtained in the absence of N_{ii} should be regarded as a common manifestation of these two components. Moreover, the nature of the ultrasound action is obviously the same for both mechanisms, which confirms that these centers differ only by location. Note that this similarity between the AI variation in a_N and a_{Lat} can also have a common initial physical component. For example, μ_N and μ_{Lat} are equally sensitive to AI increases in carrier scattering resulting from inhomogeneities and the inclusion of a secondary Te phase.

As can be seen from Table II, for satisfactory agreement of the approximation curves and $\mu_H^{exp}(T)$, we use a_{Lat} that also exhibits a certain correlation with the dislocation structure of the sample. An increase in both a_{Lat} and Δa_{Lat}^{US} values is observed as N_{Dis}^{X} increases. Undoubtedly, the degree of sample heterogeneity is manifested in the absolute value of a_{Lat}.[6,7,20,38,39] Indeed, since the regions of the electric field around the inhomogeneities are electron-impenetrable, the effective dimensions of the crystal and, respectively, the measured mobility are understated.

Some samples having different defect structures made it possible to compare the results of ultrasonic action with the features of a particular sample. In fact, one can distinguish two effects of ultrasound appearing at various temperature intervals and differing in ultrasound character. At HT, a_{Lat} increases. At LT, the opposite occurs: the lattice mechanism of electron scattering can be neglected, and the scattering on N_{ii} and N_{dc} decreases with ultrasound. As a result, N_N increases. In fact, the ultrasonic effects are determined by the complicated AI reconstruction of PD complexes within NDC, as evidenced by the long two-component σ time relaxation at LT.[13,14]

In samples with large values of N_{Dis}^{XR} (sample nos. 3, 4), a high concentration of charged centers appears. This leads to a significant scattering of charge carriers and low μ_{exp} in initial samples. Just the presence of N_{ii} and/or N_{dc} promotes effective AI growth of μ_{exp} corresponding to a decrease in their concentration (N_{ii} in the bulk and N_{dc} in the NDC). In general, these processes can occur both by deionization of the donor centers $N_D^+ + e^- \rightarrow N_D^0$ and by ionization of carriers from acceptor traps $N_A^- \rightarrow N_A^0 + e^-$. Since under US $n(T)$ increases slightly, we must assume that the last process is more probable. In particular, when turning US on, the transformation of an acceptor complex $[(V_{Cd}^{2-}Cl_{Te}^{+})^{-}]$ into a neutral $[(V_{Cd}^{2-}2Cl_{Te}^{+})^{0}]$ concomitant with temporary diffusion of Cl^+ is probable.[14]

Therefore, electron exchange processes occur between dislocation levels, conduction bands, and energy levels of surrounding local centers as a result of AI forced oscillations in the sample.[40] A portion of electrons can be transferred from the dislocation levels into a conduction band, while simultaneously increasing, albeit slightly, their non-equilibrium concentration in the conduction band. A slight $\Delta n^{US}(T)$ increase may be associated with this process under US (see Fig. 2). Electron-free (ionized) traps transform into neutral traps and increase the total N_N.

Note that, because of the "rich" defects present in our samples, it is difficult to accurately evaluate the contributions of various scattering mechanisms. However, we believe the analysis of approximated experimental curves $\mu_{exp}(T)$ and establishment of the relative AI changes enable evaluation of the main characteristics and mechanisms of the AI changes in the EPh parameters of $Cd_{1-x}Zn_xTe$ samples.

CONCLUSIONS

We have studied the temperature-dependent (77–300 K) behavior of the electron concentration and mobility by the Hall method under ultrasound (the acoustic Hall method) to determine the mechanism by which ultrasound influences the electrical conductivity $\sigma(T)$ in low-ohmic $Cd_{1-x}Zn_xTe$ ($N_{Cl} \approx 10^{24}$ m^{-3}, $x = 0$; 0.04) n-type single crystals with various dislocation densities $N_{Dis}^{XR} = (0.4–6) \times 10^{10}$ m^{-2}. We observed the dynamic (completely inverse) influence of US, which differed for samples with different defect structures. We used a differential evolution method, which enabled estimation of the relative contribution of each scattering mechanism and its changes under US. We have analyzed experimental $\mu_H^{exp}(T)$ with nonlinear approximation of the characteristic temperature dependence for various possible scattering mechanisms of charge carriers (lattice scattering, ionized impurity scattering, neutral impurity scattering, and dislocation scattering). We found that the main mechanisms of electron scattering include not only lattice scattering, but also scattering by dislocations and ionized impurities. The latter mechanism occurs at $T < 200$ K.

Thus, using the acoustic Hall method, we found that the AI changes in the EPh parameters in the

$Cd_{1-x}Zn_xTe$ single crystals are related to the AI rearrangement of the sample defect structure that occurs mainly in NDC. The unique ability of the methodology to control the state of PD structure by dislocation intermediaries with simultaneous control of EPh semiconductor parameters holds potential for applications directed toward studying the electronic properties of complex electrically active dislocation systems in other semiconductor structures, especially those with high dislocation concentration (thin films, epitaxial nanostructures, etc.).

The results presented outline only the general (but indicative) features of AI effects in $Cd_{1-x}Zn_xTe$ single crystals. Further study of a specialized subset of samples is warranted. We believe that the theoretical basis of scattering requires further refinement for dislocation clusters of high density, particularly systems under US. Certainly, acoustic-dislocation effects do not exhaust the AI processes in these semiconductor crystals.

ACKNOWLEDGEMENTS

We express our gratitude to the employees of Chernivtsi National University, M. I. Ilashchuk, A. A. Parfenyuk, and K. S. Ulyanytskyi for supplying us with CdZnTe samples for research, and to Dr. W. H. Kozyrski at the Bogolubov Institute for Theoretical Physics for useful discussion. We are also grateful to the employees of the Institute of Semiconductor Physics of the NASU V. P. Klad'ko and N. V. Safryuk for x-ray measurements of dislocation characteristics.

REFERENCES

1. K.G. Anand, *Int. J. Eng. Manag. Sci. (IJEMS)* 4, 113 (2013).
2. L. Xu, W. Jie, X. Fu, G. Zha, T. Feng, R. Guo, T. Wang, Y. Xu, and Y. Zaman, *Nucl. Instrum. Methods Phys. Res. A* 767, 318 (2014).
3. S.I. Pekar, *Fiz. Tverd. Tela.* 8, 1115 (1966).
4. K. Guergouri, Y. Marfaing, R. Triboulet, and A. Tromson-Carli, *Rev. Phys. Appl.* 25, 481 (1990).
5. I. Turkevych, R. Grill, J. Franc, E. Belas, P. Hoschl, and P. Moravec, *Semicond. Sci. Technol.* 17, 1064 (2002). https://doi.org/10.1088/0268-1242/17/10/305.
6. P. Fochuk, Y. Nykoniuk, Z. Zakharuk, O. Kopach, N. Kovalenko, A.E. Bolotnikov, and R.B. James, *IEEE Trans. Nucl. Sci.* 64, 2725 (2017). https://doi.org/10.1109/TNS.2017.2748700.
7. V.D. Popovych, F.F. Sizov, O.A. Parfenjuk, and Z.F. Tsybrii, *Semicond. Sci. Technol.* 25, 035001 (2010). https://doi.org/10.1088/0268-1242/25/3/035001.
8. D.V. Korbutyak, S.W. Mel'nychuk, E.V. Korbut, and M.M. Borysyk, *Cadmium Telluride: Impurity-Defect States and Detector Properties* (Kyiv: Ivan Fedorov, 2000) (in Ukrainian).
9. A.I. Vlasenko, Ya.M. Olikh, and R.K. Savkina, *Semiconductors* 33, 398 (1999). https://doi.org/10.1134/1.1187701.
10. Ya.M. Olikh and M.D. Tymochko, *Tech. Phys. Lett.* 37, 37 (2011). https://doi.org/10.1134/S106378501101007X.
11. O. Olikh and K. Voytenko, *Ultrasonics* 66, 1 (2016). https://doi.org/10.1016/j.ultras.2015.12.001.
12. V. Babentsov, S.I. Gorban, I.Ya. Gorodetskiy, N.E. Korsunskaya, and M.K. Sheinkman, *Sov. Phys. Semicond.* 25, 1243 (1991).
13. Ya.M. Olikh and M.D. Tymochko, *Superlattices Microstruct.* 95, 78 (2016). https://doi.org/10.1016/j.spmi.2016.04.038.
14. Ya.M. Olikh and M.D. Tymochko, *Ukr. J. Phys.* 61, 381 (2016). https://doi.org/10.15407/ujpe61.05.0381.
15. A. Maurel, F. Lund, F. Barra, and V. Pagneux, *Int. J. Bifurc. Chaos* 19, 2765 (2009). https://doi.org/10.1142/S0218127409024475.
16. M.I. Ilashchuk, A.A. Parfenyuk, and K.S. Ulyanitskyi, *Ukr. J. Fiz.* 31, 126 (1986).
17. A.V. Savitsky, O.A. Parfenyuk, M.I. Ilashchuk, P.M. Fochouk, and N.D. Korbutyak, *Semicond. Sci. Technol.* 15, 263 (2000).
18. I.A. Gerko, V.I. Khrupa, V.P. Klad'ko, E.N. Kislovskii, and V.N. Merinov, *Ind. Lab-USSR* 54, 65 (1988).
19. M.A. Moram and M.E. Vickers, *Rep. Prog. Phys.* 72, 036502 (2009).
20. X. Zhou, D.K. Ward, B.M. Wong, F.P. Doty, and J.A. Zimmerman, *J. Phys. Chem. C* 116, 17563 (2012).
21. E.V. Kuchis, *Galvanomagnetic Effects and Investigation Methods* (Moscow: Radio i svjaz', 1990) (in Russian).
22. K. Seeger, *Semiconductor Physics* (Wien: Springer, 1973).
23. V.L. Bonch-Bruevich and S.G. Kalashnikov, *Semiconductor Physics* (Moscow: Nauka, 1977) (in Russian).
24. I.L. Shul'pina, V.V. Ratnikov, and O.A. Matveev, *Phys. Solid State* 43, 579 (2001).
25. K. Alfaramawi, *J. Ovonic Res.* 12, 147 (2016).
26. B. Segall, M.R. Lorenz, and R.E. Halsted, *Phys. Rev.* 129, 2471 (1963).
27. M. Akarsu, S. Aydogu, O. Ozbas, and S. Karakaya, *J. Non Oxide Glasses* 3, 61 (2011).
28. D. Esseni and F. Driussi, *IEEE Trans. Electron Dev.* 58, 2415 (2011).
29. S.A. Medvedev, eds., *Physics and Chemistry of II–VI Compounds* (Moscow: Mir, 1970) (in Russian).
30. K. Wang and M. Ye, *Solid State Electron.* 53, 234 (2009).
31. O.Ya. Olikh, *J. Appl. Phys.* 118, 024502 (2015).
32. R. Karthik, P.U. Sathyakam, and P.S. Mallick, *Nat. Sci.* 3, 812 (2011).
33. D.C. Look and J.R. Sizelove, *Phys. Rev. Lett.* 82, 1237 (1999).
34. V. Gopal and S. Gupta, *IEEE Trans. Electron Dev.* 50, 1220 (2003).
35. O.Ya. Olikh, A.M. Gorb, R.G. Chupryna, and O.V. Pristay-Fenenkov, *J. Appl. Phys.* 123, 161573 (2018). https://doi.org/10.1063/1.5001123.
36. A.V. Sachenko, A.E. Belyaev, N.S. Boltovets, R.V. Konakova, Ya.Ya. Kudryk, S.V. Novitskii, V.N. Sheremet, J. Li, and S.A. Vitusevich, *J. Appl. Phys.* 111, 083701 (2012).
37. O. Malyk and S. Syrotyuk, *Comput. Mater. Sci.* 139, 387 (2017).
38. M.V. Alekseenko, E.N. Arkadyeva, and A.A. Matveev, *Sov. Phys. Semicond.* 4, 349 (1970).
39. B.I. Shklovskii and A.L. Efros, *Electronic Properties of Doped Semiconductors* (Berlin: Springer, 1984).
40. Yu.A. Osipyan, eds., *Electronic Properties of Dislocations in Semiconductors* (Moscow: Editorial URSS, 2000) (in Russian).